Polymer Chemistry

Catalyst-free, aza-Michael polymerization of hydrazides: polymerizability, kinetics, and mechanistic origin of an α-effect

Journal:	*Polymer Chemistry*
Manuscript ID	PY-ART-08-2019-001199.R1
Article Type:	Paper
Date Submitted by the Author:	03-Oct-2019
Complete List of Authors:	Love, Dillon; University of Colorado Boulder, Chemical and Biological Engineering; Kim, Kangmin; University of Colorado Boulder, Chemistry Domaille, Dylan; Colorado School of Mines, Chemistry; Williams, Olivia; University of Colorado Boulder, Chemical and Biological Engineering Stansbury, Jeffrey; University of Colorado, Department of Chemical and Biological Engineering Musgrave, Charles; University of Colorado, Department of Chemical and Biological Engineering Bowman, Christopher; University of Colorado, Department of Chemical and Biological Engineering

Catalyst-free, aza-Michael polymerization of hydrazides: polymerizability, kinetics, and mechanistic origin of an α-effect

Received 00th January 20xx,
Accepted 00th January 20xx

DOI: 10.1039/x0xx00000x

Dillon Love,[a] Kangmin Kim,[b] Dylan W. Domaille,[c] Olivia Williams,[a] ,Jeffrey Stansbury,[a,d,e] Charles Musgrave,[a,b,d] and Christopher Bowman.*[,a,b,d]

ADespite the powerful nature of the aza-Michael reaction for generating C–N linkages and bioactive moieties, the bis-Michael addition of 1° amines remains ineffective for the synthesis of functional, step-growth polymers due to the drastic reduction in reactivity of the resulting 2° amine mono-addition adduct. In this study, a wide range of commercial hydrazides are shown to effectively undergo the bis-Michael reaction with divinyl sulfone (DVS) and 1,6-hexanediol diacrylate (HDA) under catalyst-free, thermal conditions to afford moderate to high molecular weight polymers with M_n = 3.8-34.5 kg mol^{-1}. The hydrazide-Michael reactions exhibit two distinctive, conversion-dependent kinetic regimes that are 2nd-order overall, in contrast to the 3rd-order nature of amines previously reported. The mono-addition rate constant was found to be 37-fold greater than that of the bis-addition at 80 °C for the reaction between benzhydrazide and DVS. A significant majority (12 of 15) of the hydrazide derivatives used here show excellent bis-Michael reactivity and achieve >97% conversions after 5 days. This behavior is consistent with calculations that show minimal variance of electron density on the N-nucleophile among the derivatives studied. Reactivity differences between hydrazides and hexylamine are also explored. Overall, the difference in reactivity between hydrazides and amines is attributed to the adjacent nitrogen atom in hydrazides that acts as an efficient hydrogen-bond donor that facilitates intramolecular proton-transfer following the formation of the zwitterion intermediate. This effect not only activates the Michael acceptor but also coordinates with additional Michael acceptors to form an intermolecular reactant complex.

Introduction

The aza-Michael addition of a N-nucleophile (donor) to an electron-deficient alkene (acceptor), is one of the most common transformations for generating C–N bonds and is used in the production of important chemical moieties, such as β-aminocarbonyls and N-containing heterocycles that are present in many antibiotics, pharmaceutics, and other bioactive molecules.[1–5] Most research on this reaction class focuses on catalytic asymmetric additions with stereo- and regio-selectivity,[6–8] improving yields of weak nucleophilic amines,[9–13] and methodology development for simple, environmentally friendly reactions that are solvent- and/or catalyst-free.[13–17] Aza-Michael reactions have received less attention than the thiol-Michael reaction for the synthesis of functional macromolecules.[18] Nevertheless, the polymerizations of diamines with bis-functional acrylates, maleimides, acrylamides, and vinyl sulfones have been used to prepare linear step-growth polymers that bind proteins,[19] that have anti-tumor activity[20] or that act as degradable pro-drug conjugates,[21] gene-transfection agents,[22] pH responsive protein delivery carriers,[23] and anticorrosion adhesives.[24] Additionally, the aza-Michel reaction is also used for post-polymerization modifications,[25–28] to fabricate thermosets,[29–34] deliver hydrogels,[26,30,35,36] generate silicon-based macromolecules,[28] and synthesize a diverse range of functional biomaterials.[37]

Linear polymers generated from the bis-Michael addition of 1° amines (RNH_2) with difunctional Michael acceptors are appealing due to the wide variety of amine derivatives available that would allow a high degree of side-chain functionality that is not achievable using most synthetic polymerization techniques. Unfortunately, the synthesis of species larger than short oligomers via bis-Michael-addition of 1° amines is challenging due to the significantly higher steric demand of the N-nucleophile following the 1st addition. Consequently, the resulting 2° amine exhibits drastically reduced kinetics for the 2nd addition, which results in poor yields of the bis-addition product, particularly under equimolar concentrations of amine and acceptor.[38–41]

Recently, we demonstrated that the aza-Michael polymerization of a 1° hydrazide, *tert*-butyl carbazate (**H12**), with divinyl sulfone (DVS) under catalyst-free, thermal conditions in DMSO generated high molecular weight (M_n = 17.0 kg mol^{-1}) step-growth polymers with pendant Boc-groups that could be post-synthetically removed to liberate reactive

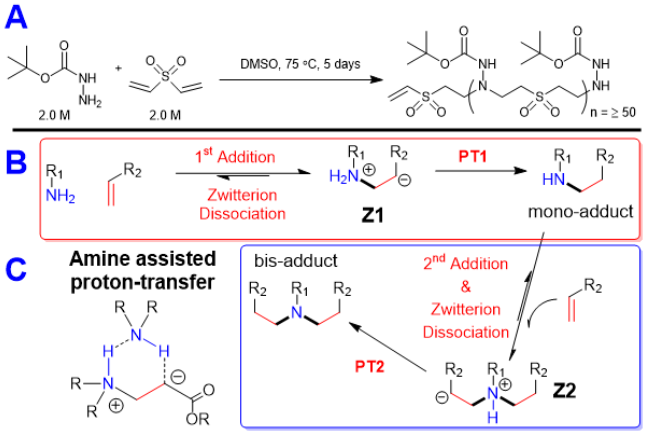

Fig. 1 (A) Previously studied hydrazide-Michael polymerization of tert-butyl carbazate with DVS.42 (B) Mechanism for the bis-aza-Michael reaction. (C) Transition state for the amine assisted proton-transfer reaction in alkyl amine-Michael reactions.

[a.] *Department of Chemical and Biological Engineering,* [b]*Department of Chemistry, and* [d]*Materials Science and Engineering Program, University of Colorado Boulder, Boulder, Colorado 80309, United States*
[c.] *Department of Chemistry, Colorado School of Mines, Golden, Colorado 80401, United StatesAddress here.*
[d.] *School of Dental Medicine, Craniofacial Biology, University of Colorado Denver, Aurora, Colorado 80045, United States*
†Electronic Supplementary Information (ESI) available: [details of any supplementary information available should be included here]. See DOI: 10.1039/x0xx00000x

hydrazine functionalities (Fig. 1a).[42] Moreover, the polymerization of **H12** with DVS delivered higher molecular weight polymers and higher conversions compared to polymerization of 1° alkylamines. In our previous work, we found that alkylamines preferentially formed cyclized products with DVS, even under solvent-free conditions. The higher polymerization efficiency of the hydrazide was attributed to the presence of a lone-pair containing heteroatom adjacent to the nucleophilic nitrogen (N_{Nu}), which is thought to enhance nucleophilicity by stabilizing the transition state (TS) through a currently unknown mechanism.[43–50] This phenomenon is known as the α-effect and is defined as the positive deviation of the α-nucleophile from a Brønsted-type plot of log k_{nuc} vs. pK_a constructed for a series of related nucleophiles.[51] Thus, we postulated that a wide-range of hydrazide derivatives that are both simple to synthesize and often commercially inexpensive would be polymerized efficiently with bis-Michael acceptors. These moieties have demonstrated uses for immobilizing biomolecules, drug-delivery, heavy metal ion removal, covalent adaptable networks, tailorable polymeric scaffolds, etc.[42,52–63] Therefore, polyhydrazide polymers have great potential as functional and modifiable polymers.

The polymerization mechanism (Fig. 1B) proceeds via two sequential nucleophilic additions, each of which consists of two elementary steps: the pseudo-equilibrated nucleophilic addition of the hydrazide to the terminal vinyl carbon that generates a zwitterionic intermediate (**Z1** or **Z2**), followed by a rate-limiting, irreversible proton-transfer (PT) reaction that affords either the mono- or bis-adduct.[40,41] Experimental and computational studies of the Michael addition of amines in aprotic polar solvents show that the lowest energy path for PT occurs via a Grotthus-like mechanism in which an external amine shuttles the proton through a 6-atom cyclic TS (Fig. 1C).[40,41,64] Additionally, these studies showed that secondary amines react more slowly than primary amines due to the increased steric hinderance of **Z2** relative to **Z1**. The increased steric demand of **Z2** decreases the thermodynamic stability of the intermediate by preventing access of the solvent to the cationic center as well as slowing the rate of PT by blocking the assisting amine from the TS.[40]

Herein, the general polymerizability/bis-aza-Michael reactivity of 15 commercially available hydrazides was explored in reactions with DVS and 1,6-hexanediol diacrylate (HDA) (Fig. 2) by monitoring polymerization rates and molecular weight distributions via ^{1}H NMR and gel permeation chromatography (GPC). The kinetics and energetics of the polymerizations were evaluated experimentally and computationally to compare quantitatively the 1st and 2nd addition steps, as well as to understand the difference in hydrazide reactivity relative to amines. A combination of experimental polymerization studies, small molecule model reactions, and quantum chemical computational studies were used to understand the tendency of hydrazides to undergo intermolecular bis-addition with DVS while 1° amines exhibited a proclivity to cyclize rapidly upon the 1st addition.

Results and discussion

Hydrazide Polymerizability

Polymerization conditions were used according to those previously optimized for the **H12**/DVS polymerization.[42] We previously reported that the greatest degree of polymerization is achieved when initial hydrazide and DVS concentrations are ≥ 2.0 M in DMSO and reacted at 75 °C for five days. Other studies on aza-Michael additions of amines also report that the kinetics are greatly enhanced by polar aprotic solvents, like DMSO and DMF, as these solvents more effectively stabilize the zwitterionic intermediate.[38–40] We also reported that the presence of additives, such as basic amines and nucleophilic phosphenes, resulted in reduced reaction efficiency.[42] Therefore, catalyst-free conditions were concluded to be optimal.

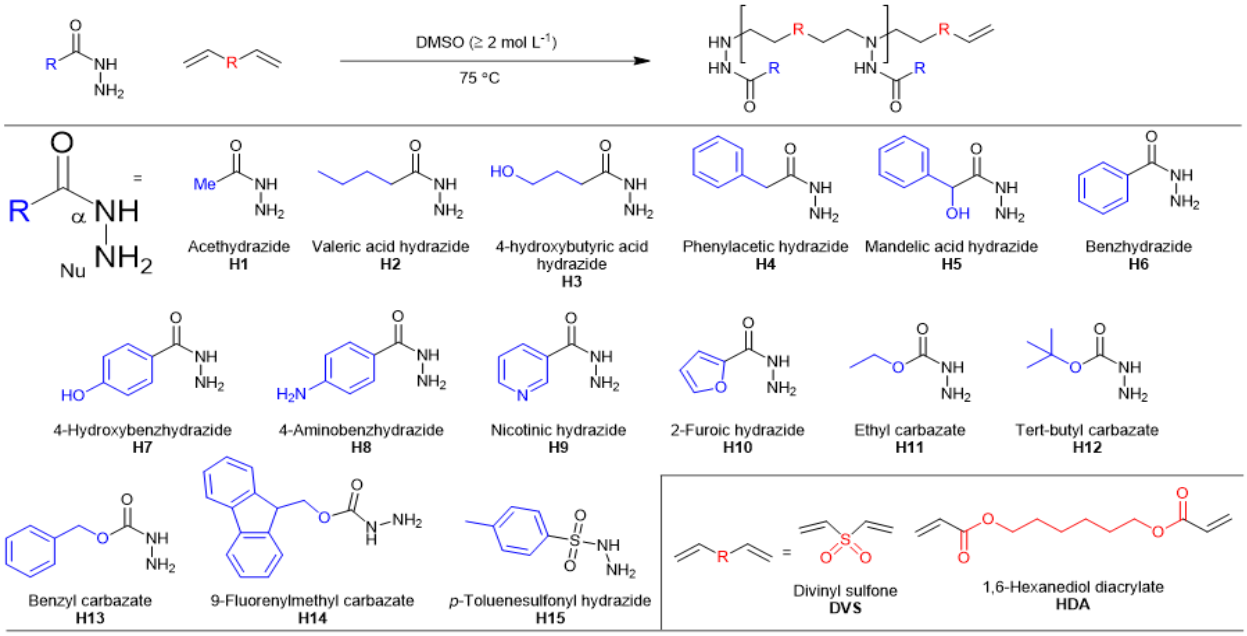

Fig. 2 Chemical structures and acronyms of hydrazides and Michael acceptors employed as monomers in this study.

Table 1 Molecular weight distribution data for the polymerizations of hydrazides with DVS[a]

Hydrazide	M_n (Da)	DP_n [b]	Đ
H1	11,500	92	1.81
H2	*c*	*c*	*c*
H3	3,900	33	1.75
H4	12,200	91	1.38
H5	10,600	75	1.48
H6	12,900	100	1.41
H7	34,500	260	1.37
H8	16,000	36	1.47
H9	*c*	*c*	*c*
H10	*c*	*c*	*c*
H11	12,900	120	1.48
H12	17,000 ‡	140	1.53
H13	10,000	71	1.59
H14	*c*	*c*	*c*
H15	*c*	*c*	*c*

[a] Molecular weight distribution data were determined via GPC (DMSO as eluent at 50 °C) using poly(methyl methacrylate) calibration. [b] $DP_N = 2*M_n/(M_{hydrazide}+M_{DVS})$. [c] Did not polymerize after five days.

Table 2 Molecular weight distribution data for the polymerizations of hydrazides with HDA[a]

Hydrazide	M_n (g mol^{-1})	DP_n [b]	Đ
H1	3,800	25	1.46
H2	c	C	c
H3	7,100	41	1.67
H4	7,300	39	1.58
H5	4,400	22	1.72
H6	5,900	33	1.74
H7	8,900	47	1.59
H8	7,700	41	1.91
H9	9,600	53	1.41
H10	5,700	32	1.61
H11	8,100	49	1.70
H12	9,500	53	1.83
H13	6,300	32	1.60
H14	c	c	c
H15	c	c	c

[a] Molecular weight distribution data were determined via GPC (DMSO as eluent at 50 °C) using poly(methyl methacrylate) calibration. [b] $DP_n = 2*M_n/(M_{hydrazide}+M_{DVS})$. [c] Did not polymerize after five days.

Here, polymerizations were carried out between commercially obtained hydrazides **H1-15** with DVS and HDA, where monomers were used as received and the initial concentrations of hydrazide and difunctional Michael acceptor were ≥ 2.0 M (depending on hydrazide solubility). Hydrazides were chosen to enable exploration of the compatibility of a wide range of side-chain functionalities, including aliphatic, aromatic, basic (**H8-10**), acidic (**H3**, **H5**, **H7**), as well as several hydrazides with amine protecting groups that could be post-synthetically removed to liberate reactive hydrazines (**H12-14**). Polymerizations were performed over 5 days and were monitored periodically with ^{1}H NMR and GPC of the crude reaction mixtures (final GPC traces of the crude polymerization mixtures are shown in Figs. S3&4). The final molecular weight distribution data of the main polymer peaks obtained after 120 h are reported in Tables 1 and 2 for DVS and HDA polymers, respectively. Ten hydrazides afforded polymers with DVS resulting in M_n = 3.9-34.5 kg mol^{-1} and number-average degree of polymerizations (DP_n) = 33-260, corresponding to theoretical conversions of 97% to >99% and polydispersities (Đ) ranging from 1.38 to 1.81 suggesting the mechanism deviates significantly from ideal step-growth behaviour which would predict polydispersities to be 1.97 to 2.00. Most likely, this deviation is the result of the enhanced reactivity of the unsubstituted 1° hydrazide versus the mono-substituted 2° hydrazide that leads to the exclusive formation of trimers and dimers until the 1° hydrazide species are consumed, followed by the formation of higher molecular weight species as the bis-addition proceeds. ^{1}H NMR analysis of the final reaction mixture after 120 h revealed the complete disappearance of the DVS vinyl protons at 7.1 (1H) and 6.3 ppm (2H), (Fig. S1). Failure of **H9** and **H10** to polymerize with DVS was attributed to the insolubility of the nascent low molecular weight oligomers, evidenced by both hydrazides initially being soluble followed by the evolution of precipitate prior to 24 h. NMR and GPC analysis showed only monomer remaining in the solution phase of the reaction mixture. Other solvent systems were explored for the polymerization of **H9** and **H10**; however, these were unsuccessful due to the poor solubility of hydrazides in other solvents, such as THF, acetonitrile, methanol, water, and DCM. Although DMF seemed promising due to its ability to dissolve most hydrazides, attempts to polymerize **H1**, **H4**, **H6**, **H9**, **H10**, **H12**, and **H13** with DVS in DMF at 75 °C yielded poor conversions (<80% for all cases) due to precipitation of oligomers within 10 h of reacting. The reaction of **H15** with DVS and HDA likely resulted in a crosslinked polymer, as evidenced by the generation of insoluble precipitate within 10 h and the absence of starting materials in solution phase, as determined by ^{1}H NMR and GPC. This behaviour was attributed to the thermal degradation of the *p*-toluenesulfonyl hydrazide linkage, liberating a highly reactive tetrafunctional hydrazine species. Reducing the temperature prevented the precipitation event but only 74% conversion of the DVS vinyl groups was achieved after reacting for a week at 21 °C, well below the near quantitative extent of reaction that is necessary to generate viable molecular weight polymer via step-growth reactions. Realizing functional linear polymers from **H15** would likely require the incorporation of a catalyst that enables the polymerization at near-ambient conditions.

Twelve hydrazides afforded moderate molecular weight polymers with HDA, M_n = 3.8-9.6 kg mol^{-1} and DP_n = 22-53, corresponding to theoretical conversions from 95 to 98%. All hydrazides that polymerized with DVS showed good polymerizability with HDA, in addition to **H9** and **H10**. The improved solubility of some hydrazide-HDA polymers in the reaction solution, in contrast to their DVS counterparts, is attributed to the hexyl alkyl spacer between carbonyl moieties, which reduces H-bonding site density along the polymer chain, decreases backbone rigidity, and is more organophilic than the DVS moiety. The potential aminolysis of the HDA ester by the hydrazide was dismissed as a side-reaction due to previous computational work by Desmet et al., that showed nucleophilic

attack to the terminal alkene to be much more favored than attacking the carbonyl carbon for the reaction of ethylamine and diethylamine with ethyl acrylate.[40]

Comparison of the carbamate-type(carbazate) (**H11**-**14**) to the amide-type hydrazide reactions reveal no discernable differences in the general reactivity of the two subclasses. This observation is consistent throughout the kinetic studies presented later in this manuscript. Additionally, calculations of the electronic nature of individual hydrazides (vide infra) reveal that the electronic density on N_{Nu} is equivalent out to two significant figures regardless of being an amide- or carbamate-type and the substituent structure.

H2, **H3**, and **H14** have bulky aliphatic substituents and exhibited lower reactivities. **H2** and **H14** were the only hydrazides that did not polymerize with either DVS or HDA. It is expected that the large aliphatic moieties reduce reactivity by increasing the steric effects that hinder both the addition and PT steps, as well as further limiting the interaction of DMSO solvent molecules with the **Z1** and **Z2** cationic centers.[40] Increasing the reaction temperature to 120 °C over the course of 7 days yielded no appreciable increase in rate or molecular weight. Previously, we observed that when **H12** was reacted with DVS at ≥100 °C, nonspecific degradation of the polymer was observed to occur after 24 h.[42] To determine whether this thermal instability was ubiquitous among hydrazide-Michael polymers, polymerizations of **H4**, **H6**, and **H13** with DVS and HDA were performed at 120 °C for 7 days and were observed to proceed normally with no discernable degradation via NMR and GPC analysis (Fig. S5). This observation greatly increases the applicability of these and similar hydrazide-Michael type polymers. The observed instability of **H12** polymers may be attributed to the thermally labile nature of the Boc group rather than the instability of the aza-Michael linkage or hydrazide functional group.[65]

Hydrazide **H7** exhibited significantly enhanced polymerizability with DVS, achieving >99% vinyl conversion after 10 h and DP_n = 86, 170, and 260 after 24, 48, and 120 h, respectively. Due to the presence of the hydroxyl functional group on the **H7** substituent, we hypothesized that the oxa-Michael side-reaction may be occurring simultaneously leading to hyperbranched polymers and larger hydrodynamic volume species affecting GPC measurements. To investigate this possibility, **H7** and other hydrazides with potential Michael donor groups (**H3**, **H5**, and **H8**) were reacted off-stoichiometrically with DVS and HDA at 75 °C for 7 days with a 50% molar excess of diene. ^{1}H NMR analysis showed that the final ratio of hydrazide side-groups to unreacted vinyl functional groups was 1:1 for all reactions, corresponding to the one-to-one reaction of hydrazides with diene and a lack of vinyl consuming side-reactions. Likewise, GPC traces of the reaction products (Fig. S6) reveal only the presence of four discrete low molecular weight products. Although fortuitous, the lack of oxa-Michael reactions in **H3** and **H7** polymerizations is surprising given that the anion present on **Z1** and **Z2** could potentially deprotonate the hydroxy groups to afford the reactive alkoxide anion during reactions with both HDA and DVS.[66–69] This suggests that the zwitterion intermediates are relatively short-lived and that the free energy pathway for hydroxy deprotonation is significantly higher than for proton-transfer. Further, the enhanced reactivity of **H7** could be a result of the phenol hydroxy group acting as a Brønsted-type Lewis acid catalyst by H-bonding with the carbonyl on the Michael-acceptor to increase the vinyl reactivity.[10,16,70,71] Additionally, polymerizations of **H6** with DVS and HDA were conducted in a H_2O/DMSO mixture (1:10 H_2O:DMSO by volume) to see if the rate or conversion are affected by water. Although the reaction rate was slightly reduced compared to a pure DMSO solvent environment, the kinetic rate constants were still within a standard error of the original reactions, and quantitative conversion was still achieved after 5 days for both reactions.

Hydrazide-Michael Polymerization Kinetics

H4, **H6**, and **H13** polymerizations were selected for further analysis of the hydrazide-Michael kinetics and energetics because these substrates span the three main types of hydrazides studied: alkyl, aryl, and alkyl ether substituted amides, the latter of which is defined as the carbazate sub-class of hydrazides. Vinyl conversions (Fig. 3) and molecular weight evolution (Fig. 4 for **H4**, Fig. S7 for **H6** and **H13**) versus time were monitored by ^{1}H NMR and GPC analysis of the crude reaction mixture over the course of 5 days (Fig. S1, S2). The three hydrazides displayed similar reactivity, with most of the reaction taking place within 1 h and reaching ≥98% conversion

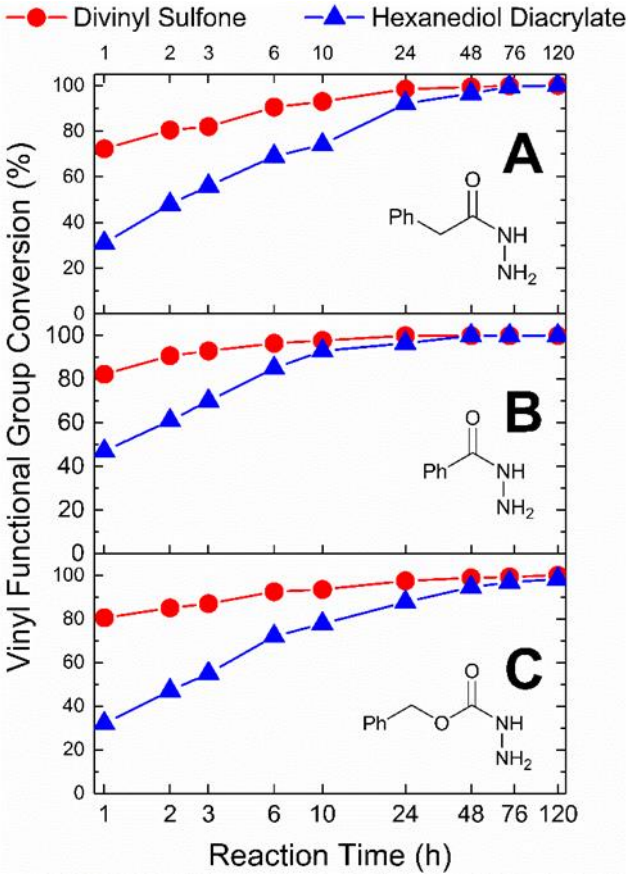

Fig. 3 Vinyl functional group conversion versus time for the polymerization of (A) **H4**, (B) **H6**, and (C) **H13** with DVS and HDA over five days. Conversions were determined via ^{1}H NMR.

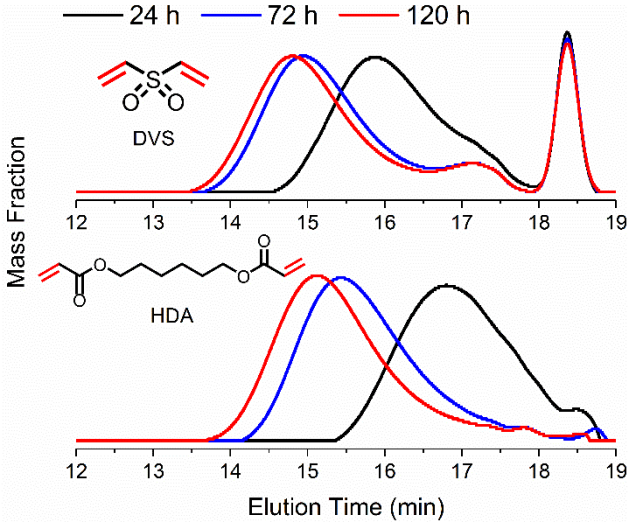

Fig. 4 GPC traces of the crude reaction mixture for the polymerizations of **H4** with DVS and HDA over the course of five days.

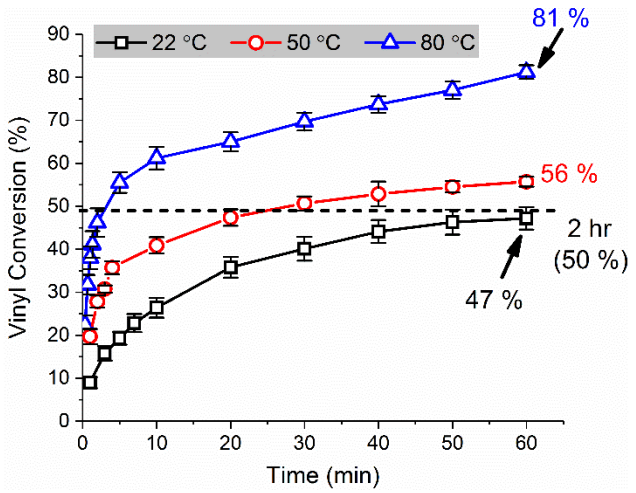

Fig. 5 Vinyl functional group conversion versus time for the reaction of **H6** with DVS at different temperatures. Conversions were determined via ^{1}H NMR.

within 24 h for DVS reactions. This result is captured by the GPC traces that show the emergent polymeric species after 24 h, followed by moderate increases of M_n after 3 and 5 days. HDA polymerizations were substantially slower, reaching only 31-47% conversion after 1 h but still reaching >99% conversion within 2 (**H6**) to 5 (**H4**, **H13**) days. Molecular weight distribution profiles of DVS and HDA derived polymers exhibit distinctive characteristics. In general, DVS polymers afford trimodal distributions, in which the largest (71 to 84 wt%) polymer peak is attributed to the high molecular-weight polymeric species. This assignment is informed by previous work that showed the main polymer peak to be isolable for the **H12**/DVS polymer through washing. The two other peaks correspond to the 6-atom cyclization product (~18.3 min) and cyclized oligomers (16.50 to 17.75 min), respectively.[42] Conversely, HDA polymers are monomodal due to the fourteen atom spacing between the terminal carbons of the vinyl functional groups that precludes cyclization events.

Next, the apparent rate constants for the mono-adduct (k_1) and bis-adduct (k_2) formations were determined. Temperature dependencies of the **H6** and **H12** reactions with DVS were evaluated by monitoring the reactions over the course of an hour at 22, 50, 70, and 80 °C (Fig. 5, Fig. S13). Vinyl conversions for both reactions at 22 °C asymptotically approach 50% corresponding to the complete transformation of the hydrazide into the mono-adduct and indicate that the 2nd addition is insignificant on the hour time scale at this temperature. GPC traces taken during the **H6**/DVS reaction at 22 °C confirm that species larger than dimer and trimer emerge only at conversions surpassing 50% (Fig. S8). This outcome also indicates that the intramolecular, 6-atom cyclization reaction also requires thermal activation. Upon raising the temperature, the reactions readily exceed 50% conversion, and the bis-addition product appears. To determine the reaction order in vinyl and hydrazide functionalities, several plausible rate expressions were considered, and their corresponding kinetic models were compared to the experimental conversion data (SI Section 2). When evaluating model accuracy, it was assumed that the mono-addition reaction operates exclusively at less than 50% vinyl conversion. In contrast, at ≥50% conversion it was assumed that all hydrazide had been transformed to the mono-adduct, and the observed reaction corresponds to the 2nd addition. Essentially, these assumptions arise from an overall understanding that the first reaction proceeds to near completion prior to the second reaction beginning.

The most accurate model for both steps was found to be 2nd order overall, 1st order in 1° or 2° hydrazide ([RNH_2] and [R_2NH], respectively) and vinyl concentration.

$$1^{st}\text{ addition:}\quad d[\text{vinyl}]/dt = -k_1[RNH_2][\text{vinyl}] \qquad (1)$$

$$2^{nd}\text{ addition:}\quad d[\text{vinyl}]/dt = -k_2[R_2NH][\text{vinyl}] \qquad (2)$$

Where $[RNH_2] = [\text{vinyl}] - [RNH_2]_0$ for the 1st addition, $[R_2NH] = [\text{vinyl}]$ for the 2nd addition, $[RNH_2]_0$ is the initial hydrazide concentration (2 M), and $[\text{vinyl}]_0$ is the initial concentration of vinyl functional groups (4 M). Integrating the differential expressions results in the following relations between vinyl concentration versus time (t):

1° addition:

$$\ln\left[\frac{[\text{vinyl}]-[RNH_2]_0}{[\text{vinyl}]}\right] = -k_1[RNH_2]_0 t - \ln\left[\frac{[\text{vinyl}]_0-[RNH_2]_0}{[\text{vinyl}]_0}\right] \qquad (3)$$

2° addition:

$$1/[\text{vinyl}] = k_2 t + 1/[\text{vinyl}]_0 \qquad (4)$$

Application of these derived linear transformations to the 1st and 2nd addition reactions of H6 are shown in Figs. 6 and 7, respectively, and for the H12 reactions in Figs. S14 and S17, respectively.

In contrast to the kinetic results obtained here, previous studies on amine-Michael addition in polar aprotic solvents and under solventless conditions displayed 3rd-order overall kinetics: 2nd-order in amine, and 1st-order in vinyl

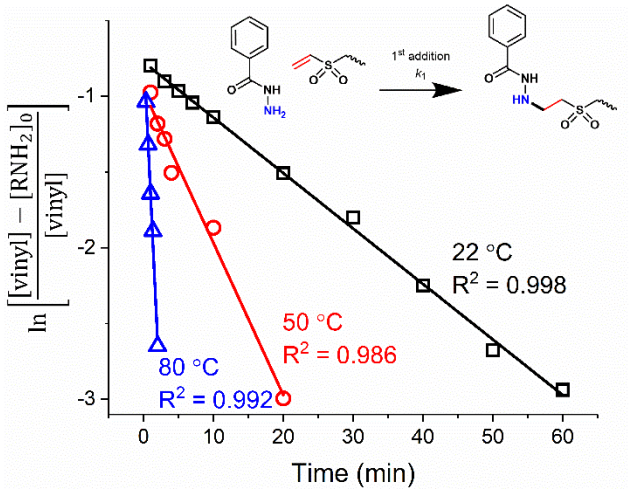

Fig. 6 Linear fit of vinyl conversion data versus time for the mono-addition reaction of **H6** with DVS according to the 2nd-order reaction model solution, shown in Equation 3.

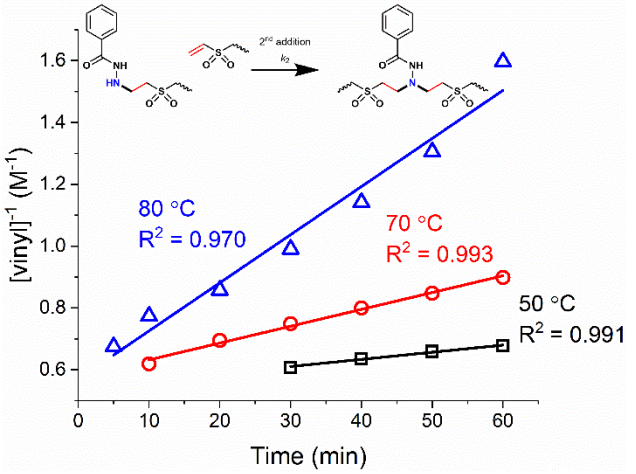

Fig. 7 Linear fit of vinyl conversion data versus time for the bis-addition reaction of **H6** with DVS according to the 2nd-order reaction model solution, shown in Equation 4.

concentration. This difference is a result of the addition step being pseudo-equilibrated and PT being rate-limiting and occurring through the amine-assisted pathway.[38,40,41] Assuming that the addition step is still pseudo-equilibrated due to the endergonic nature of the reaction and the resultant unstable zwitterionic intermediate, the PT step is also expected to remain rate-limiting for hydrazide-Michael reactions, which implies that the hydrazide derived zwitterion undergoes unimolecular PT without the involvement of an additional hydrazide. Desmet et al. showed that intramolecular PT is possible in amine reactions through a 4-atom cyclic TS but that the free energy barrier for this process is significantly greater than the amine-assisted pathway (~13 kcal mol^{-1} difference). Therefore, a lower free energy path for intramolecular PT must exist for hydrazide zwitterion adducts than for the typical alkyl amine adducts. The most plausible mechanism is illustrated in Fig. 8, in which the initial PT event occurs via a 5-atom TS between the N–H of the amide motif and the carbanion, resulting in an iminolate that deprotonates the cationic ammonium group through another 5-atom TS. Finally, the formed iminol undergoes tautomerization to the amide structure, facilitated by the high concentration of basic amino groups in solution. To test the feasibility of this mechanism, TS energies and the thermodynamics of each step were calculated for the **Z1** intermediate for acethydrazide (**H1**) reacting with methyl vinyl sulfone. The 1st PT is effectively barrierless and irreversible ($\Delta G^{\ddagger}$ = 0.5, $\Delta G°$ = -25.5 kcal mol^{-1}) due to the conversion of the highly energetic carbanion to a resonance stabilized oxyanion indicating that the addition step is irreversible as the PT should occur faster than the diffusion limit. While the 2nd PT is also nearly barrierless, the conversion of the iminolate to iminol is weakly exergonic and thus highly reversible. However, the tautomerization to form the final mono-adduct is irreversible ($\Delta G°$ = -36.4 kcal mol^{-1}). These results establish this mechanism as the exclusive PT pathway and offer rationalization of how hydrazide-Michael polymerizations achieve high DP_n, because diffusion will have no impact on the PT rate, and PT will readily continue to occur when all amino species capable of assisting have been converted into the bis-adduct. Further, this mechanism explains the lack of oxa-Michael side reaction described herein and suggests the reaction could be performed in the presence of alkyl thiols as well. For hydrazide-acrylate reactions, intramolecular PT occurs through the same mechanism as for vinyl sulfones as well as by deprotonation of N_α or N_{Nu} by the oxyanion of the enolate tautomer through a 7- or 6-atom TS. The latter two cases would result in the neutral 1,4-addition adduct, but this enol is predicted to undergo irreversible tautomerization to the 1,2-addition ketone adduct based on calculations by Desmet et al.[40]

To obtain 2nd order kinetic constants and apparent activation energies of the 1st addition ($E_{a,1}$) for **H4**, **H6**, **H12**, and **H13** with DVS and HDA (Table 3), 1:1 stoichiometric reactions were conducted at 22, 30, 40, 50, 60, 70, and 80 °C for DVS reactions and 50, 60, 70, and 80 °C for HDA reactions. Aliquots of the crude reactions mixtures were analyzed using ^{1}H NMR at short time intervals to minimize the 2nd addition contribution to the observed rates by ensuring that vinyl conversions were held under 50%. Activation energies were determined using the Arrhenius relationship by determining the best-fit slope of ln(k_1) versus 1/T (Fig 9). DVS reactions exhibit reactivities up to 40- to 70-fold greater than the corresponding HDA reactions at 80 °C, but only a 2-fold difference exists in reactivity amongst the slowest and fastest hydrazides for both DVS and HDA reactions. All four hydrazide reactions with DVS have activation energies that are not statistically different over the range of 60 to 80 °C, but variation is much more pronounced for HDA reactions. For example, E_{a1} for the **H12**/HDA reaction is ~30% of E_{a1} for the **H6**/HDA. Accordingly, it would be expected that **H12** is significantly more reactive with HDA than **H6**; however, in reality, the reaction of **H12** with HDA is marginally faster at 60 °C compared to **H6**, while **H6** is two-fold faster at 80 °C.

The reaction of **H12** with DVS (Fig. 10) and HDA (Fig. S20) appear to have two temperature-dependent kinetic regimes with significantly different activation energies for the mono-addition step. For the DVS and HDA reactions, at T = 22-50 °C and T = 50-70 °C, respectively, the E_{a1} values are equivalent out

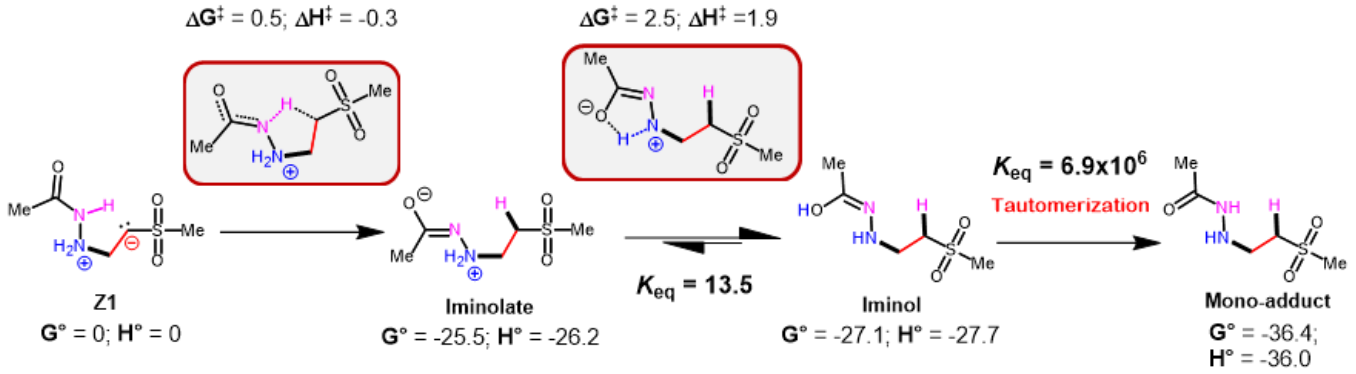

Fig. 8 Mechanism for intramolecular proton-transfer in hydrazide-Michael reactions. Calculated enthalpy and free energy values are reported in kcal mol^{-1}.

Table 3 Kinetic constants and energetics of the 1st addition

Ene	Hydrazide	k_1 (L·mol^{-1}·hr^{-1})[a] 60 °C	k_1 (L·mol^{-1}·hr^{-1})[a] 80 °C	Apparent Activation Energy (kcal·mol^{-1})[b] $E_{a,1}$	Vinyl Group Conversion (%)[c] 1 hr at 75 °C
DVS	**H4**	5.0 ± 0.1	15.1 ± 0.7	12.5 ± 0.5	72
	H6	9.4 ± 0.9	31 ± 1	12.8 ± 0.6	82
	H12[d]	10 ± 1	24.7 ± 0.4	11 ± 1	69
	H12[e]	"	"	5.3 ± 0.6	"
	H13	5.4 ± 0.6	23 ± 1	13 ± 1	81
HDA	**H4**	0.10 ± 0.03	0.36 ± 0.04	16.7 ± 0.4	31
	H6	0.17 ± 0.02	0.78 ± 0.12	16 ± 2	47
	H12[f]	0.19 ± 0.02	0.41 ± 0.08	5.3 ± 0.7	36
	H13	0.13 ±0.06	0.34 ± 0.07	11 ± 1	32

[a]k_1 calculated assuming that the primary addition of the hydrazide with DVS is the only contribution to vinyl conversion. [b]Activation energy determined for reactions between 22 and 80 °C.for DVS reactions and between 50 and 80 °C for HDA reactions. [c]Conversions were determined by proton NMR. [d]Activation energy determined for reactions between 60 and 80 °C. [e]Activation energy determined for reactions between 22 and 50 °C. [f]Activation energy determined for reactions between 50 and 70 °C.

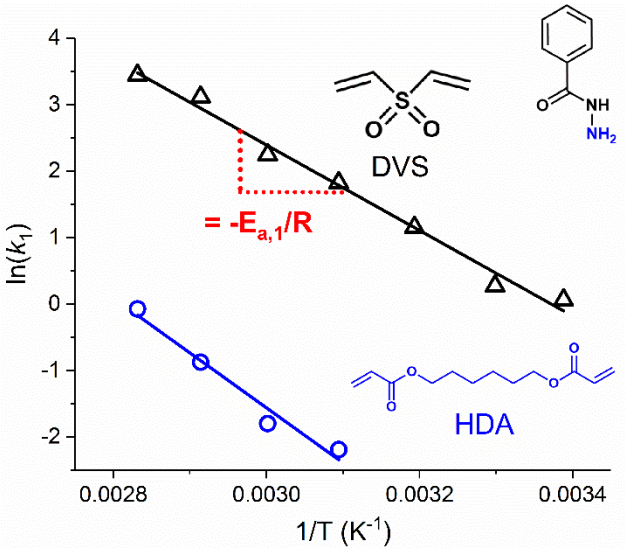

Fig. 9 Arrhenius plots of the dependence of k_1 on temperature for the reaction of **H6** with DVS and HDA.

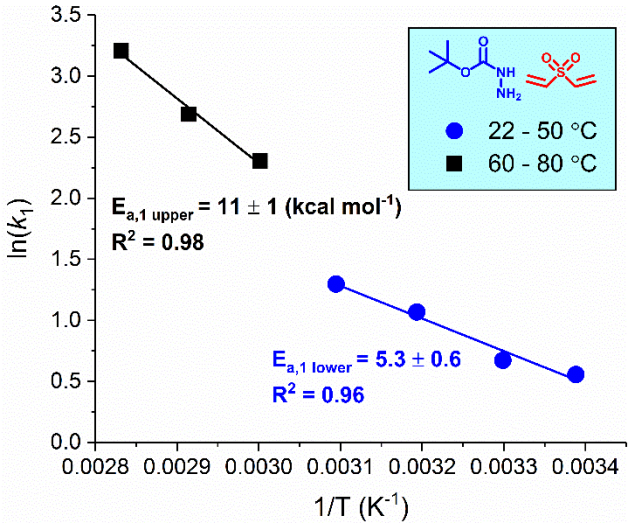

Fig. 10 Arrhenius plots of the dependence of k_1 on temperature for the reaction of **H12** with DVS

to two significant figures (5.3 kcal mol^{-1}), which is greatly reduced compared to the activation energies observed for all other hydrazide-Michael reactions studied. Increasing temperature above those ranges leads to the emergence of kinetic constants significantly larger than predicted from extrapolating the Arrhenius relationship. In the case of **H12**/DVS, the higher T regime displays an $E_{a,1}$ value two-fold greater than at low T. Although not testable here due to the high freezing point of DMSO (19 °C), the other hydrazide reactions may possess a high to low activation energy kinetic

regime transition that is not observable under these experimental conditions.

The activation energy for the 2nd addition of the **H6**/DVS reaction was calculated to be 14.5 kcal mol^{-1} (Fig. S21), only a 1.7 kcal mol^{-1} increase over $E_{a,1}$, and k_1(80 °C) was 33-fold larger than k_2(80 °C), 0.94 versus 31 L mol^{-1} hr^{-1}, respectively. Likewise, k_1 is 43-fold larger than k_2 at 80 °C for the **H12**/DVS reaction. The kinetics of the **H6**/DVS and **H12**/DVS reactions were simulated using equations 1 and 2 and the experimentally determined kinetic parameters to predict the vinyl functional group conversion profiles (see SI section 4 for simulation details and analysis). The model predictions are consistent with the observed conversions profiles (Fig S22 and S23) and upon further analysis affirm that the bis-addition reaction rate is less than 5% of the mono-addition rate until 1° hydrazide conversion reaches 57% at 80 °C (77% at 22 °C, see Fig S25). Reaction selectivities for the formation of the mono- versus bis-substituted product as a function of 1° hydrazide conversion were also modeled (Fig S26), predicting that for temperatures between 22 and 80 °C the mono-adduct is favored 10 to 1 until the 1° hydrazide conversion surpasses 95% and that at 22 °C the mono-adduct is favored 100 to 1 until >66% 1° hydrazide conversion. Overall, both experimental and model results justify the treatment of the mono- and bis-additions as conversion separated regimes during kinetic analysis, especially at temperatures near ambient. Further, the reaction differences between the 1st and 2nd additions are more pronounced near room temperature; thus, the bis-addition potentially could be selectively initiated by increasing the reaction temperature to make hydrazide-Michael reactions ideal for asymmetric additions on the N-center or selectively synthesizing mono-addition products using only temperature as the reaction control. Based on both the simulated kinetics, ^{1}H NMR analysis, low activation energies, and large thermodynamic driving force for adduct formation presented here in, it is expected that the dominant limiting factor for polymer molecular weight evolution is the degree at which equal stoichiometry of reactants is achieved since monomers were used as received, particularly for the hydrazide-vinyl sulfone reaction.

Computational results

To understand further the Michael reactivity of hydrazides, the effects of substituent structure on this reactivity and to expand the scope of this subclass of Michael reactions, the electronic structures of the reactants and the reaction energetics of the 1st and 2nd additions were studied for the reactions of **H2**, **H4**, **H6**, **H12**, and **H13** with DVS and n-propyl acrylate (nPA, chosen as a model for HDA to reduce the computational expense of the calculations). To mimic the nature of the reaction medium, geometry optimizations to determine the molecular structures were performed in a simulated solvent environment described using the universal solvation model (SMD) with parameters chosen to describe DMSO.[72] These studies focused on understanding the anomalous lack of reactivity of **H2**, the enhanced reactivity of DVS, and to discern any correlations between the hydrazide substituent and the electronic and or reactive nature of the –NHNH$_2$ functionality.

Initially, the electron densities of the two Michael-acceptors and five hydrazides were evaluated, as reported in Tables 4 and 5, respectively. This assessment was motivated by the fact that for structurally similar electrophiles and nucleophiles their reactivity differences are accurately estimated using the energy of the electrophile's lowest unoccupied molecular orbital (LUMO) and the energy of the nucleophile's highest occupied molecular orbital (HOMO).[73,74] Generally, a lower energy LUMO and higher energy HOMO result in better orbital overlap and increased stabilization of the TS, i.e., a smaller HOMO-LUMO gap corresponds to a lower activation enthalpy. Furthermore, the reactivity of electrophiles can be ordered based on Parr's electrophilicity index ω, where $\omega = \mu^2/2\eta$, μ is the chemical potential and η is the chemical hardness.[75] This analysis may partly explain the observed reactivity differences between the vinyl sulfone and acrylate functionalities, where the vinyl sulfone possesses a lower LUMO energy by 0.11 eV and a higher ω by 0.06 eV. Additionally, the predicted partial charges on the terminal and internal vinyl carbons of DVS and nPA were evaluated. In contrast to nPA, which has equal electron density on each vinyl carbon, DVS possesses a large dipole moment where the localized electron density is 0.18 lower on the terminal carbon than the internal carbon. This phenomenon arises from greater delocalization of charge through the conjugated acrylate functional group, which the tetrahedral S-centered sulfone lacks. The presence of the dipole moment may act to further enhance DVS's reactivity by directing the nucleophilic attack to the more electron deficient terminal carbon.

Table 4 Electronic properties of DVS and nPA

	Electron density of vinyl carbons			
Acceptor	$C_{terminal}$	$C_{internal}$	LUMO (eV)	ω (eV)
DVS	-0.36	-0.54	-0.75	1.42
nPA	-0.36	-0.36	-0.64	1.36

Table 5 Electronic properties of nucleophiles

	Electron Density			
Hydrazide	N_{Nu}	N_α or C_α	$C_{carbonyl}$	HOMO (eV)
H2	-0.76	-0.52	0.68	-8.18
H4	-0.76	-0.52	0.69	-7.54
H6	-0.76	-0.52	0.67	-7.93
H12	-0.76	-0.55	0.94	-8.22
H13	-0.76	-0.55	0.93	-7.84
Hexylamine	-0.73	0.53	N/A	-7.64

In contrast to the acceptors, hydrazide substituents are predicted to have a minimal effect on the electronic structure. Hydrazides were predicted to have a range of HOMO energies from -7.84 to -8.22 eV, but we found no correlation between their computed HOMO energies and the experimentally obtained values of k_1 and E_{a1}. The calculated electron densities on the primary N_{Nu} and N_α atoms are nearly equivalent across the five hydrazides, indicating that the carbonyl functionality

acts as an electronic buffer between the substituent and –$NHNH_2$ motifs. Therefore, the reactivity differences must arise from differences in the thermodynamics of the **Z1**/**Z2** formation steps that arise from steric effects, solvation effects, distortion effects,[76] and potentially pre-transition state coordination of the reactants.

We also evaluated the energetics of the mono- and bis-addition steps using a benzhydrazide (**H6**) and DVS model chemistry and found that the TS energies lie within 1 kcal mol^{-1} of the **Z1** and **Z2** energies (Table S1). These results suggest a late transition state with significant bond formation. Therefore, the TS energies for the other three hydrazide reactions with DVS and HDA were approximated by the energies of the zwitterionic intermediates.

Overall, our calculations predict that the 1st and 2nd addition steps are highly thermodynamically favorable (ΔG° = -18.9 and -18.8 kcal mol^{-1} for the mono- and bis-adduct of **H6** with DVS, respectively) in contrast to the formation of **Z1** from the reaction of **H2**, **H4**, **H6**, **H12**, and **H13** with DVS and HDA, which is endergonic by 15-18 and 17-21 kcal mol^{-1}, respectively. This difference again favors reaction with DVS, in agreement with experimental observations. Interestingly, **Z2** formation for the reaction of **H6** with DVS and HDA is predicted to be approximately 4.5 and 10.5 kcal mol^{-1} less endothermic than for **Z1** formation, as the first adduct to N_{Nu} inductively donates electron density that increases the nucleophilicity and provides more stabilization of the positive charge upon addition. Given these predictions that reaction electronic properties of hydrazides and calculated reaction energetics vary minimally with hydrazide derivatization, we hypothesized that the lack of observed reactivity for **H2** and **H14** is a result of their substituents having low rotational barriers that lead to an ensemble of conformers at a given temperature, affecting the activation free energies and the TS population. It was recently reported that omitting the presence of conformers can lead to a significant overestimation of computationally calculated rate constants even with small alkyl groups (ethyl vs methyl) when compared to experimental results.[77] Although the **H12** substituent may be considered bulky, we expect that its reactivity is relatively unhindered due to the symmetric nature of the *tert*-butyl group resulting in degenerate conformations and the O–C bond being the only mode for conformational change.

Bis-Michael addition reactivity of hydrazides versus 1° amines

In the initial study of hydrazide polymerizations with DVS, the polymerization of several 1° amines were also attempted under identical conditions. It was observed that allyl amine and hexylamine preferentially underwent intramolecular bis-addition to afford a 6-atom cyclized product and no high molecular weight polymeric species.[1] Additionally, 1° amines often require amine or acceptor activating catalysts (i.e., Lewis bases or Lewis acids, respectively), high T, and excess acceptor to achieve quantitative conversion,[4] which is in stark contrast to the behavior of most of the hydrazides presented here when reacting with vinyl sulfones and acrylates. To explore this difference further, model small molecule reactions of **H6** and hexylamine with the monofunctional Michael-acceptors ethyl vinyl sulfone (EVS), hexyl acrylate (HA), and diethyl maleate (DEM) were conducted in DMSO at 75 °C for 5 days with two equivalents of acceptor (Table 6). ^{1}H NMR spectrums of the crude reaction solutions were taken after 1, 24, and 120 h to determine vinyl consumption. For both nucleophiles, reactions with DEM achieved 50% conversion within an hour but conversion only marginally increased at 120 h. These reactions undergo only mono-addition due to the increase in the steric restriction afforded by the DEM adduct, despite its highly electron deficient nature. **H6** achieved quantitative conversions with EVS and HA after 120 h while reaction with hexylamine proceeded to nearly quantitative conversions with EVS but only 65% conversion with HA. Although the hydrazide reaction with EVS proceeded faster than with hexylamine over the course of an hour, hexylamine achieved a significantly higher conversion with HA at 1 h, but subsequently the reaction slowed drastically beyond the 50% conversion mark. Hexylamine was also reacted with stoichiometric DVS and HDA under the standard hydrazide polymerization conditions. The reaction of hexyl amine and DVS was noticeably exothermic, and vapor was observed. In contrast, such extreme reactivity was not observed for any hydrazide reaction. The reaction proceeded for 5 days, and analysis of the crude hexylamine/DVS reaction by GPC showed only the formation of short oligomers with DVS (Fig. S28), despite obtaining 100% vinyl conversion. These results clearly demonstrate that hydrazides are more reactive towards the bis-addition, particularly with acrylates, but the reactivity towards the mono-addition is highly substrate dependent. Furthermore, the preference of hydrazides for intermolecular bis-addition over the formation of the highly favorable 6-atom intramolecular adduct suggests strong intermolecular complexation between the hydrazide mono-adduct and another vinyl sulfone functional group.

Table 6 Reactivity comparison of benzhydrazide (**H6**) and hexylamine with monofunctional Michael-acceptors[a]

		Vinyl group conversion (%)[b]		
Acceptor	Nucleophile	1 h	24 h	120 h
Ethyl vinyl sulfone	**H6**	63±4	96±1	Quant.[c]
(EVS)	Hexylamine	47±5	87±5	Quant.
Hexyl acrylate	**H6**	40±2	88±3	Quant.
(HA)	Hexylamine	51±1	56±1	65±3
Diethyl maleate	**H6**	51±2	53±1	55±1
(DEM)	Hexylamine	52±2	54±1	57±1

[a] Reactions were conducted at 75 °C in DMSO, [acceptor] = 2*[nucleophile] = 4 M. [b] Conversions determined by ^{1}H NMR of the crude reaction mixtures. [c] ≥ 99% conversion.

To understand the contrasting behaviors between amine and hydrazide, we first examined their electronic properties (Table 5) and found that the energy of the amine HOMO lies within the range of the calculated hydrazides and that the electron density on N_{Nu} is similar to that of the hydrazides. This result agrees with our previous conclusion that Michael

reactivity differences among N-nucleophiles cannot be reliably predicted from electronic structure characteristics alone. Although the presence of an inductively donating alkyl functionality would be expected to stabilize the positive charge located on N_{Nu} at the TS of addition and the zwitterion intermediate, the partial negative charge on N_{α} indicates the presence of lone-pair character that may enhance nucleophilicity of hydrazides through the α-effect.[43–48,50] Because the mechanistic origins of the α-effect remain elusive in the literature, an explicit explanation for the differences in hydrazide/amine reactivities was desired. We hypothesized that the presence of an efficient H-bond donating amide/carbamate moiety adjacent to N_{Nu} produces an amino functional group that forms strong H-bonding complexes in comparison to typical 1° alkyl amines. Strong H-bonding may allow the hydrazide to form a pre-transition state complex with DVS and HDA that could then direct hydrazides to react intermolecularly while also activating DVS and HDA via Lewis acid catalysis. This hypothesis about the effect of catalytic H-bonding is well-supported in the literature as H-bonds have often been used to catalyze nucleophilic additions and direct their stereochemistry.[13,49,78–80] To demonstrate the feasibility of this mechanism, the optimized H-bond complex structures were calculated (Fig. 11A and B) for dimethyl sulfone with ethyl substituted acethydrazide and diethyl amine in order to mimic the mono-adduct aza-Michael products. The hydrazide complex with two distinct H-bonds is observed to be 5.3 kcal mol^{-1} more stable in free energy than the isolated species, while the amine complex with a single H-bond is 3.7 kcal mol^{-1} more stable. Such strong H-bond coordination may potentially play several roles in the increased bis-reactivity and preference for the intermolecular reaction with DVS. Additionally, the additional H-bonding site away from N_{Nu} in hydrazides suggests that the hydrazide motif retains its catalytic activity upon conversion to the bis-addition product, opening up the possibility of using polyhydrazide materials of the type studied here to be used as recoverable, homogenous-phase catalysts for less reactive aza-Michael systems.

H-bond mediated 6-atom cycles with a chair conformation are also predicted to occur at the transition states for **Z1** (Fig S27) and **Z2** (Fig. 11C) in the reaction of **H6** with DVS due to the non-planar tetrahedral geometry of the sulfonyl group. This arrangement is not possible for the conjugated, trigonal planar geometry of the acrylate carbonyl (Fig. S27). An additional 7-atom, H-bond cycle is also possible in hydrazide-vinyl sulfone reactions; however, this possibility was not explored further. Having established that the PT occurs intramolecularly (vide supra), the H-bonding in the TS structure may act to orient the carbanion and N_{α}–H proton into the geometry required for the 5-atom PT to form the iminolate intermediate, thus reducing the entropic barrier to deprotonation. Because H-bonding is highly favorable in hydrazide-Michael reactions, it should also be expected that intramolecular H-bonding exists, in either a 6- or 7-atom configuration, in the neutral mono- and bis-adduct products. In the case of the mono-adduct, this interaction would restrict the conformational freedom of the DVS residue and thereby reduce the probability of cyclization further.

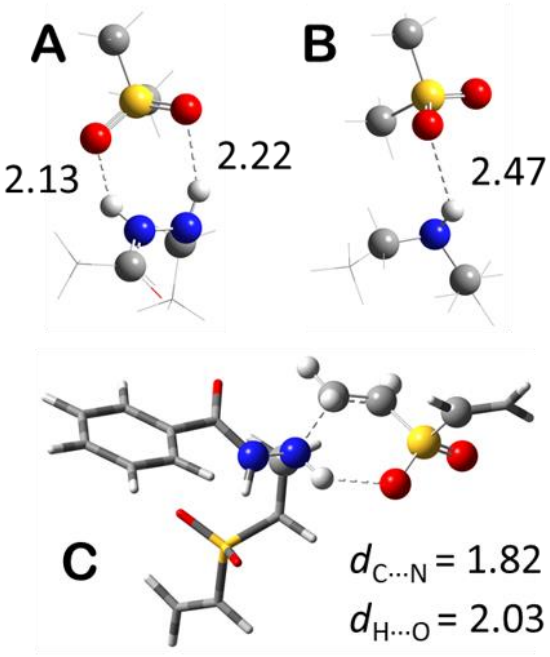

Fig. 11 Hydrogen-bond mediated complex between dimethyl sulfone and (A) mono-substitute acethydrazide (B) diethylamine. (C) DFT calculated six-atom, chair conformation transition state structure for the bis-addition reaction between **H6** and DVS. Distances are reported in angstroms.

Conclusions

In conclusion, the characteristics of the hydrazide-Michael reaction were explored with a broad array of hydrazide structures in the context of step-growth, linear polymerizations and small-molecule reactions. Despite the requirements of long reaction times for polymerization reactions, heat, and the limited range of usable solvents, this reaction class, particularly the hydrazide-vinyl sulfone addition, exhibit many of the "click" characteristics described by Sharpless in 2001:[81] facile reaction conditions and simple purification, no detectable side-reactions, full atom economy, orthogonal to other Michael donor functional groups (alcohols and amines), regioselective towards the 1,4-addition versus 1,2-addition, irreversible, insensitive to air and water, and able to be performed with a wide range of commercially cheap starting materials (hydrazides and Michael acceptors) that do not require extensive purification. Further, long reaction times are demonstrated to be necessary only for achieving the highest possible molecular weights, based on simulated kinetics and NMR conversion studies.

The kinetics, energetics, and mechanism of the hydrazide-Michael bis-addition reaction were explored for the purposes of generating high molecular-weight step-growth polymers. It was demonstrated that the hydrazide sub-class of 1° amino nucleophiles undergoes near quantitative bis-additions with vinyl sulfones and acrylates under catalyst-free, stoichiometric conditions via 2nd-order overall kinetics. Quantum chemical calculations predicted that the presence of the N heteroatom

with amide functionality alpha to the nucleophilic center facilitates significantly stronger pre-reaction coordination with divinyl sulfone relative to amine nucleophiles as well as enables the hydrazide-derived zwitterion intermediate to undergo nearly barrierless unimolecular PT to afford the neutral Michael adduct. Taken together, the combination of reaction trends and computational studies suggest that the α-effect is responsible for the superior bis-reactivity of hydrazides compared to amines. Additionally, the adjacent amide nitrogen atom is an efficient H-bond donor that may act as a Lewis acid activator for the Michael acceptor, facilitate intramolecular PT, and complex with Michael acceptors to bias the reaction towards intermolecular bis-addition with DVS rather than forming cyclized side products. Although the heteroatom lone-pair adjacent to the nucleophilic center does not explicitly contribute to the enhanced Michael reactivity of hydrazides, as is commonly assumed with α-nucleophiles, the lone-pair allows for the conjugation of N_α to afford the amide functionality that has superior H-bond donating capacity compared to amines.[82]

The overall effectiveness of hydrazide-Michael reactions enables the potential for the combinatorial synthesis of functional copolymers by incorporating multiple hydrazides with orthogonal side-group chemical reactivities and acceptors into a single reaction pot. The potential for thermally selective mono-/bis-addition should be explored in future work for asymmetric hydrazide-Michael additions, which in combination with the large monomer library, could prove attractive for synthesizing sequence-ordered copolymers. Polyhydrazides as materials may be promising as a recoverable, homogenous-phase catalyst with dual Lewis acid and Lewis base character for Michael reactions, which could be enhanced by incorporating hydrazides with appropriate side-chain functional group chemistries. Additionally, due to the highly bioactive nature of hydrazides as well as their strong tendency to hydrogen bond and interact with metals, copolymers prepared from hydrazide-Michael reactions have great potential as biocidal and other pharmaceutical materials,[52,58,63] telechelic oligomers for the preparation of mechanically tough thermosets,[83,84] covalent adaptable networks,[55,85] or materials for the filtration of heavy metals.[56,57,61]

Experimental

Materials and general methods

All chemicals used for this study were obtained commercially and used as received. Divinyl sulfone (97%, contains ≤500 ppm hydroquinone as inhibitor), 1,6-hexanediol diacrylate (99% reactive esters with 90 ppm hydroquinone), valeric acid hydrazide (95%), mandelic acid hydrazide (97%), 4-hydroxybutyric hydrazide (98%), benzhydrazide (98%), ethyl carbazate (97%), and hexyl acrylate (95%) were purchased from Alfa Aesar; acethydrazide (95+%) and *p*-toluenesulfonyl hydrazide (97%) were purchased from Matrix Scientific; phenylacetic hydrazide (>98%), 9-fluorenylmethyl carbazate (>98%), and hexylamine (>99%) were purchased from Tokyo Chemical Industry; 4-aminobenzhydrazide (95%), 2-furoic hydrazide (98%), ethyl vinyl sulfone (98%), and diethyl maleate (97%) were purchased from Sigma Aldrich; *tert*-butyl carbazate (99%) and benzyl carbazate (97%) were purchased from Oakwood Chemical; 4-hydroxybenzhydrazide (≥98%) was purchased from Chem-Impex International, Inc.; nicotinic hydrazide (97%) was purchased from Acros Organics.

Molecular weight distribution data were obtained *via* gel permeation chromatography (GPC) of the crude polymerization solutions. GPC was carried out with a TOSOH ECO SEC HLC-8320GPC equipped with two polystyrene columns and UV and refractive index detectors operating at 50 °C with DMSO as the eluent. Data were calibrated using poly(methyl methacrylate) standards. Samples were syringe filtered through 0.2 μm pore sized nylon filters purchased from Life Science Products. ^{1}H NMR spectra were acquired on a 400 MHz Bruker Avance-III spectrometer using DMSO-d_6 as the solvent and TMS as the internal reference.

General polymerization procedure. A 20 mL scintillation vial was charged with a stir bar, DVS (100.4 μL, 1.00 mmol) or HDA (224 μL, 1.00 mmol) and solution of hydrazide (1.00 mmol) in DMSO. Hydrazides were dissolved in the volume of DMSO that afforded a final reaction solution where [hydrazide] = [DVS] or [HDA] = 2.0 mol L^{-1}. For hydrazides that did not completely dissolve, DMSO/hydrazide mixtures were sonicated at 50 °C for 15 min. If the hydrazides still were not dissolved, then 100 μL of DMSO were added and sonicated again at 50 °C for 15 min. This was repeated until a homogenous solution was obtained. The reaction vial was then stirred for 120 h and heated at 75 °C.

Reaction kinetic studies. A flask was charged with a stir bar and a hydrazide (1.00 mmol) dissolved in DMSO (400 μL) and equilibrated at the reaction temperature for 10 min. Then DVS (100.4 μL, 1.00 mmol) or HDA (224 μL, 1.00 mmol) were added all at once to the stirring flask. At designated time points, 50 μL of the reaction solution was withdrawn and diluted into 500 μL of DMSO-d_6 and then immediately transferred into NMR tubes chilled in ice water until ^{1}H NMR spectra could be recorded.

Computational methods

All quantum mechanical calculations were performed within the GAUSSIAN 16 Revision A.03 software package[86] using DFT based on the MN15 density functional[87] and 6-31+G(d,p) basis set.[88] The MN15 functional was chosen because it has been extensively parameterized with experimental data and provides an accurate description of the molecular geometries.[87] Vibrational force constants were computed to verify that stationary states were optimized to their correct structures and to determine vibrational entropies, zero-point energies and thermal corrections at 298 K as well as at 378 K to account for the higher observed temperatures under reaction conditions. Solvent effects were described using the universal solvation model (SMD)[72] with parameters for dimethyl sulfoxide (DMSO) in order to match the experimental conditions. For reactions in solution, the ideal gas, rigid rotor, and harmonic oscillator approximations used in statistical mechanics calculations tend to overestimate the entropic contribution to the Gibbs free energy due to the unaccounted for inhibition of the translational and rotational motions of reactants by solvent molecules.[89] We previously used a protocol that provides more accurate entropic contributions to the energies of reaction in

polymer solutions with success.[77] In this study, we determined that Gibbs free energies modified by the exclusion of translational entropy accurately reflect the confined microscopic environment of reactions occurring in solution as we previously explained in detail in reference [77]. Electron densities were obtained via the Natural Population Analysis within the Natural Bond Orbital approach (version 3.1) as implemented in Gaussian16.[90]

Characterization of crude polymerization products

Divinyl sulfone polymers

H1/DVS. ^{1}H NMR (400 MHz, DMSO-d_6) δ 8.86 (s, 1H), 1.78-1.97 (m, 3H). IR(KBr) ν_{max} cm^{-1} 3200 (NH), 1665 (CO), 1550 (*trans* NH), 1460 (*cis* NH), 1290 and 1140 (SO_2).

H2/DVS. Did not polymerize.

H3/DVS. ^{1}H NMR (400 MHz, DMSO-d_6) δ 8.36 (s, 1H), 3.11-3.40 (m, 8H), 2.41 (m, 2H), 2.11 (m, 2H), 1.65 (m, 2H).

H4/DVS. ^{1}H NMR (400 MHz, DMSO-d_6) δ 942 (m, 1H), 7.25 (m, 5H), 3.38 (m, 2H), 2.96-3.31 (m, 8H). ^{13}C NMR (101 MHz, DMSO-d_6) δ 156.13, 137.09, 128.84, 128.38, 128.23, 66.23, 50.88, 50.10.

H5/DVS. ^{1}H NMR (400 MHz, DMSO-d_6) δ 9.22 (s, 1H), 7.44 (d, J = 7.2 Hz, 2H), 7.31 (m, 3H), 6.18 (d, J = 4.2 Hz, 1H), 4.97 (d, J = 3.1 Hz, 1H), 2.98-3.23 (m, 8H).

H6/DVS. ^{1}H NMR (400 MHz, DMSO-d_6) δ 9.48 (s, 1H), 7.77-7.79 (m, 2H), 7.38-7.55 (m, 3H), 3.23-3.43 (m, 8H). IR(KBr) ν_{max} cm^{-1} 3260 (NH), 1720 (CO), 1530 (*trans* NH), 1460 (*cis* NH), 1290 and 1150 (SO_2).

H7/DVS. ^{1}H NMR (400 MHz, DMSO-d_6) δ 10.00 (s, 1H), 9.27 (s, 1H), 7.68 (m, 2H), 6.79 (m, 2H), 3.23-3.45 (m, 8H). ^{13}C NMR (101 MHz, DMSO-d_6) δ 166.09, 160.88, 129.95, 124.28, 115.25, 51.05, 49.72.

H8/DVS. ^{1}H NMR (400 MHz, DMSO-d_6) δ 9.10 (s, 1H), 7.55 (m, 2H), 6.54 (m, 2H), 5.64 (s, 2H), 3.16-3.50 (m, 8H).

H9/DVS. Did not polymerize.

H10/DVS. Did not polymerize.

H11/DVS. ^{1}H NMR (400 MHz, DMSO-d_6) δ 8.48 (s, 1H), 4.03 (t, J = 7.0 Hz, 2H) 3.33 (m, 4H), 3.16 (m, 4H), 1.18 (t, J = 7.1 Hz, 3H).

H12/DVS. Reference 42. ^{1}H NMR (400 MHz, DMSO-d_6) δ 8.19 (s, 1H), 3.28(t, J = 7.0 Hz, 4H), 3.15 (t, J = 7.2 Hz, 4H), 1.40 (s, 9H). ^{13}C NMR (101 MHz, DMSO-d_6) δ 155.46, 79.41, 50.84, 49.98, 28.58. IR(KBr) ν_{max} cm^{-1} 3180 (NH), 1715 (CO), 1500 (*trans* NH), 1460 (*cis* NH), 1295 and 1160 (SO_2).

H13/DVS. ^{1}H NMR (400 MHz, DMSO-d_6) δ 8.60 (s, 1H), 7.26-7.42 (m, 5H), 5.04 (s, 2H), 3.24-3.38 (m, 4H), 3.11-3.22 (m, 4H). IR(KBr) ν_{max} cm^{-1} 3200 (NH), 1715 (CO), 1525 (*trans* NH), 1455 (*cis* NH), 1295 and 1140 (SO_2).

H14/DVS. Did not polymerize.

H15/DVS. Did not polymerize.

1,6-Hexanediol diacrylate polymers

H1/HDA. ^{1}H NMR (400 MHz, DMSO-d_6) δ 8.01 (s, 1H), 4.01 (m, 4H), 2.92 (m, 4H), 1.79 (m, 3H), 1.56 (m, 4H), 1.33 (m, 4H).

H2/HDA. Did not polymerize.

H3/HDA. ^{1}H NMR (400 MHz, DMSO-d_6) δ 8.57 (s, 1H), 3.99 (t, J = 6.8 Hz, 4H), 3.36 (m, 2H), 2.98 (m, 4H), 2.39 (m, 4H), 2.10 (m, 2H), 1.59 (m, 6H), 1.32 (m, 4H).

H4/HDA. ^{1}H NMR (400 MHz, DMSO-d_6) δ 8.87 (s, 1H), 7.24 (m, 5H), 3.98 (m, 4H), 3.33 (t, J = 7.3 Hz, 4H), 2.99 (t, J = 2.8 Hz, 2H), 2.39 (m, 4H), 1.54 (m, 4H), 1.29 (m, 4H). IR(CH_2Cl) ν_{max} cm^{-1} 3280 (NH), 1730 (CO, ester), 1670 (CO, hydrazide), 1420 (NH).

H5/HDA. ^{1}H NMR (400 MHz, DMSO-d_6) δ 8.78 (s, 1H), 7.42 (m, 2H), 7.30 (m, 3H), 6.03 (d, J = 5.0 Hz, 1H), 4.90 (d, J = 5.0 Hz, 1H), 3.97 (t, J = 6.8 Hz, 4H), 2.97 (t, 7.7 Hz, 4H), 2.29 (t, J = 7.8 Hz, 4H), 1.55 (m, 4H), 1.30 (m, 4H).

H6/HDA. ^{1}H NMR (400 MHz, DMSO-d_6) δ 9.18 (s, 1H), 7.79 (m, 2H), 7.47 (m, 3H), 3.93 (t, J = 6.8 Hz, 4H), 3.12 (t, J = 6.8 Hz, 4H), 2.46 (t, J = 6.8 Hz, 4H), 1.46 (m, 4H), 1.22 (m, 4H). ^{13}C NMR (101 MHz, DMSO-d_6) δ 172.18, 165.90, 134.11, 131.70, 128.63, 127.73, 64.21, 52.30, 32.74, 28.35, 25.42. IR(CH_2Cl_2) ν_{max} cm^{-1} 3250 (NH), 1730 (CO, ester), 1660 (CO, hydrazide), 1540 (*trans* NH), 1460 (*cis* NH).

H7/HDA. ^{1}H NMR (400 MHz, DMSO-d_6) δ 9.97 (s, 1H), 8.95 (s, 1H), 7.65 (m, 2H), 6.78 (m, 2H), 3.90 (t, J = 6.5 Hz, 4H), 3.09 (t, J = 6.8 Hz, 4H), 2.42 (t, J = 6.8 Hz, 4H), 1.46 (m, 4H), 1.18 (m, 4H).

H8/HDA. ^{1}H NMR (400 MHz, DMSO-d_6) δ 8.73 (s, 1H), 7.50 (d, J = 8.5 Hz, 2H), 6.52 (d, J = 8.3 Hz, 2H), 5.59 (s, 2H), 3.91 (t, J = 6.6 Hz, 4H), 3.08 (t, J = 6.9 Hz, 4H), 2.41 (t, J = 6.5 Hz, 4H), 1.48 (m, 4H), 1.22 (m, 4H).

H9/HDA. ^{1}H NMR (400 MHz, DMSO-d_6) δ 9.39 (s, 1H), 8.92 (m, 1H), 8.68 (dd, J = 4.8, 1.5 Hz, 1H), 8.11 (dt, J = 8.0, 1.7 Hz, 1H), 7.48 (dd, J = 7.9, 4.8 Hz, 1H), 3.90 (t, J = 4.0 Hz, 4H), 3.11 (t, J = 7.0 Hz, 4H), 2.47 (t, J = 7.0 Hz, 4H), 1.45 (m, 4H), 1.20 (m, 4H).

H10/HDA. ^{1}H NMR (400 MHz, DMSO-d_6) δ 9.08 (s, 1H), 7.81 (m, 1H), 7.08 (m, 1H), 6.60 (m, 1H), 3.91 (t, J = 6.6 Hz, 4H), 3.05 (t, 7.0 Hz, 4H), 2.39 (t, J = 7.0 Hz, 4H), 1.48 (m, 4H), 1.24 (m, 4H).

H11/HDA. ^{1}H NMR (400 MHz, DMSO-d_6) δ 8.06 (s, 1H), 3.98 (m, 6H), 2.93 (m, 4H), 2.39 (t, J = 7.0 Hz, 4H), 1.56 (m, 4H), 1.32 (m, 4H), 1.15 (t, J = 7.0 Hz, 3H).

H12/HDA. ^{1}H NMR (400 MHz, DMSO-d_6) δ 7.75 (s, 1H), 3.99 (t, J = 6.5 Hz, 4H), 2.89 (m, 4H), 2.38 (t, J = 7.2 Hz, 4H), 1.56 (m, 4H), 1.37 (s, 9H), 1.31 (m, 4H). IR(CH_2Cl_2) ν_{max} cm^{-1} 3230 (NH), 1730 (CO, ester and carbazate), 1460 (*trans* NH), 1420 (*cis* NH).

H13/HDA. ^{1}H NMR (400 MHz, DMSO-d_6) δ 7.96 (s, 1H), 7.33 (m, 5H), 5.01 (s, 2H), 3.97 (m, 4H), 2.93 (m, 4H), 2.40 (t, J = 7.1 Hz, 4H), 1.53 (m, 4H), 1.28 (s, 4H). ^{13}C NMR (101 MHz, DMSO-d_6) δ 172.01, 155.96, 137.46, 128.76, 128.04, 126.87, 65.61, 64.21, 52.64, 32.46, 28.43, 25.47. IR(CH_2Cl_2) ν_{max} cm^{-1} 3050 (CH, aromatic), 1730 (CO, ester and carbazate), 1440 (NH).

H14/HDA. Did not polymerize.

H15/HDA. Did not polymerize.

Conflicts of interest

There are no conflicts to declare.

Acknowledgements

We gratefully acknowledge financial support from NSF-MRSEC (DMR 1420736), DoEd GAANN program, NSF CHE-1214131, and NIH/NIDCR (R21DE028017)

Notes and references

1 1 Z. Amara, J. Caron and D. Joseph, *Nat. Prod. Rep.*, 2013, **30**, 1211–1225.
2 2 M. Sánchez-Roselló, J. L. Aceña, A. Simón-Fuentes and C. Del Pozo, *Chem. Soc. Rev.*, 2014, **43**, 7430–7453.
3 3 J. Wang, P. Li, P. Y. Choy, A. S. C. Chan and F. Y. Kwong, *ChemCatChem*, 2012, **4**, 917–925.
4 4 A. Y. Rulev, *Russ. Chem. Rev.*, 2011, **80**, 197–218.
5 5 A. Y. Rulev, *Russ. Chem. Bull.*, 2016, 65, 1687–1699.
6 6 L. W. Xu and C. G. Xia, *European J. Org. Chem.*, 2005, 633–639.
7 7 D. Enders, C. Wang and J. X. Liebich, *Chem. - A Eur. J.*, 2009, **15**, 11058–11076.
8 8 X. F. Wang, J. An, X. X. Zhang, F. Tan, J. R. Chen and W. J. Xiao, *Org. Lett.*, 2011, **13**, 808–811.
9 9 C. E. Yeom, M. J. Kim and B. M. Kim, *Tetrahedron*, 2007, **63**, 904–909.
10 10 M. H. Ghasemi, E. Kowsari and A. Shafiee, *Tetrahedron Lett.*, 2016, **57**, 1150–1153.
11 11 S. Kim, S. Kang, G. Kim and Y. Lee, *J. Org. Chem.*, 2016, **81**, 4048–4057.
12 12 T. Selvi and S. Velmathi, *J. Org. Chem.*, 2018, **83**, 4087–4091.
13 13 A. Fedotova, E. Kondrashov, J. Legros, J. Maddaluno and A. Y. Rulev, *Comptes Rendus Chim.*, 2018, **21**, 639–643.
14 14 X. Chen, X. Li, H. Song, Y. Qian and F. Wang, *Tetrahedron Lett. Int. Organ Rapid Publ. Prelim. Commun. Org. Chem.*, 2011, **52**, 3588–3591.
15 15 Z. Amara, E. Drège, C. Troufflard, P. Retailleau and D. Joseph, *Org. Biomol. Chem.*, 2012, **10**, 7148–7157.
16 16 H. L. Hou, F. L. Qiu, A. G. Ying and S. L. Xu, *Chinese Chem. Lett.*, 2015, **26**, 377–381.
17 17 R. Asgharzadeh, G. Imanzadeh and Z. Soltanzadeh, *Green Chem. Lett. Rev.*, 2017, **10**, 80–87.
18 18 C. R. Fenoli and C. N. Bowman, *Chem. Mater.*, 2014, **26**, 724.
19 19 P. Ferruti, M. A. Marchisio and R. Duncan, *Macromol. Rapid Commun.*, 2002, **23**, 332–355.
20 20 P. Ferruti, E. Ranucci, F. Trotta, E. Gianasi, G. E. Evagorou, M. Wasil, G. Wilson and R. Duncan, *Macromol. Chem. Phys.*, 1999, **200**, 1644–1654.
21 21 P. Ferruti, E. Ranucci, L. Sartore, F. Bignotti, M. A. Marchisio, P. Bianciardi and F. M. Veronese, *Biomaterials*, 1994, **15**, 1235–1241.
22 22 D. M. Lynn and R. Langer, *J. Am. Chem. Soc.*, 2000, **122**, 10761–10768.
23 23 P. C. Griffiths, A. Paul, Z. Khayat, K. W. Wan, S. M. King, I. Grillo, R. Schweins, P. Ferruti, J. Franchini and R. Duncan, *Biomacromolecules*, 2004, **5**, 1422–1427.
24 24 M. Han, H. Bie, D. E. Nikles and G. W. Warren, *J. Polym. Sci. Part A Polym. Chem.*, 2000, **38**, 2893–2899.
25 25 E. S. Read, K. L. Thompson and S. P. Armes, *Polym. Chem.*, 2010, **1**, 221–230.
26 26 C. Hoffmann, M. C. Stuparu, A. Daugaard and A. Khan, *J. Polym. Sci. Part A Polym. Chem.*, 2015, **53**, 745–749.
27 27 A. Narayanan, B. Maiti and P. De, *React. Funct. Polym.*, 2015, **91–92**, 35–42.
28 28 A. Genest, D. Portinha, E. Fleury and F. Ganachaud, *Prog. Polym. Sci.*, 2017, 72, 61–110.
29 29 M. Retailleau, A. Ibrahim, C. Croutxé-Barghorn, X. Allonas, C. Ley and D. Le Nouen, *ACS Macro Lett.*, 2015, **4**, 1327–1331.
30 30 T. Tang and A. Takasu, *RSC Adv.*, 2015, **5**, 819–829.
31 31 R. Baruah, A. Kumar, R. R. Ujjwal, S. Kedia, A. Ranjan and U. Ojha, *Macromolecules*, 2016, **49**, 7814–7824.
32 32 M. Retailleau, A. Ibrahim, C. Croutxé-Barghorn and X. Allonas, *RSC Adv.*, 2016, **6**, 47130–47133.
33 33 A. O. Konuray, X. Fernández-Francos, À. Serra and X. Ramis, *Eur. Polym. J.*, 2016, **84**, 256–267.
34 34 M. Retailleau, A. Ibrahim, C. Croutxé-Barghorn and X. Allonas, *Prog. Org. Coatings*, 2016, **100**, 51–55.
35 35 A. Southan, M. Mateescu, V. Hagel, M. Bach, C. Schuh, C. Kleinhans, P. J. Kluger, S. Tussetschläger, I. Nuss, T. Haraszti, S. V. Wegner, J. P. Spatz, H. Boehm, S. Laschat and G. E. M. Tovar, *Macromol. Chem. Phys.*, 2013, **214**, 1865–1873.
36 36 J. Wang, H. He, R. C. Cooper and H. Yang, *ACS Appl. Mater. Interfaces*, 2017, **9**, 10494–10503.
37 37 W. Cheng, D. Wu and Y. Liu, *Biomacromolecules*, 2016, **17**, 3115–3126.
38 38 B. W. G. Davies, E. W. Hardisty, T. P. Nevell, R. H. Peters and F. Science, *J. Chem. Soc.*, 1970, 1004–1007.
39 39 L. T. T. Nguyen, M. T. Gokmen and F. E. Du Prez, *Polym. Chem.*, 2013, **4**, 5527–5536.
40 40 G. B. Desmet, D. R. D'hooge, P. S. Omurtag, P. Espeel, G. B. Marin, F. E. Du Prez and M.-F. Reyniers, *J. Org. Chem.*, 2016, **81**, 12291–12302.
41 41 M. Blaha, O. Trhlikova, J. Podesva, S. Abbrent, M. Steinhart, J. Dybal and M. Duskova-Smrckova, *Tetrahedron*, 2018, **74**, 58–67.
42 42 D. W. Domaille, D. M. Love, X. Y. Rima, A. Harguindey, B. D. Fairbanks, D. Klug, J. N. Cha and C. N. Bowman, *Polym. Chem.*, 2018, **9**, 3791–3797.
43 43 J. E. Dixon and T. C. Bruice, *J. Am. Chem. Soc.*, 1971, **93**, 3248–3254.
44 44 J. E. Dixon and T. Bruice, *J. Am. Chem. Soc.*, 1972, **94**, 2052–2056.
45 45 I. Um, J. Lee, S. Bae and E. Buncel, *Can. J. Chem.*, 2005, **1371**, 1365–1371.
46 46 I. Um, Y. Shin, J. Han and E. Buncel, *Can. J. Chem.*, 2006, **1556**, 1550–1556.
47 47 Y. Ren and H. Yamataka, *J. Org. Chem.*, 2007, **72**, 5660–5667.
48 48 T. A. Nigst, A. Antipova and H. Mayr, *J. Org. Chem*, 2012, **77**, 8142–8155.
49 49 R. Ormazabal-Toledo, R. Contreras, R. A. Tapia and P. R. Campodonico, *Org. Biomol. Chem.*, 2013, **11**, 2302–2309.
50 50 E. T. Kool, P. Crisalli and K. M. Chan, *Org. Lett.*, 2014, **16**, 1454–1457.
51 51 P. Muller, *Pure Appl. Chem.*, 1994, **66**, 1077–1184.
52 52 D. Horák, M. Karpíšek, J. Turková and M. Beneš, *Biotechnol. Prog.*, 1999, **15**, 208–215.
53 53 E. A. Hoff, B. A. Abel, C. A. Tretbar, C. L. McCormick and D. L. Patton, *Polym. Chem.*, 2017, **8**, 4978–4982.
54 54 D. N. Crisan, O. Creese, R. Ball, J. L. Brioso, B. Martyn, J. Montenegro and F. Fernandez-Trillo, *Polym. Chem.*, 2017, **8**, 4576–4584.
55 55 S. Debnath, R. R. Ujjwal and U. Ojha, *Macromolecules*, 2018, **51**, 9961–9973.
56 56 R. Liu, B. Zhang and H. Tang, *Fresenius. J. Anal. Chem.*, 1998, **362**, 258–262.
57 57 A. M. Gad, A. El-Dissouky, E. M. Mansour and A. El-Maghraby, *Polym. Degrad. Stab.*, 2000, **68**, 153–158.
58 58 V. V Shmani, T. A. Nikolayeva, L. G. Vinokurova and A. A. Litoshka, *BMC Biotechnol.*
59 59 G. S. Liou, S. H. Hsiao and S. U. Tzy-Hsiang, *J. Polym. Sci. Part A Polym. Chem.*, 2005, **43**, 3245–3256.
60 60 K. Godula and C. R. Bertozzi, *J. Am. Chem. Soc.*, 2010, **132**, 9963–9965.
61 61 I. S. bt Johari, N. A. Yusof, M. J. Haron and S. M. Mohd Nor, *Polymers (Basel).*, 2013, **5**, 1056–1067.

62 62 A. Kumar, R. R. Ujjwal, A. Mittal, A. Bansal and U. Ojha, *ACS Appl. Mater. Interfaces*, 2014, **6**, 1855–1865.
63 63 R. R. Ujjwal, M. P. Purohit, S. Patnaik and U. Ojha, *ACS Appl. Mater. Interfaces*, 2015, **7**, 11506–11507.
64 64 C. H. Lim, A. M. Holder and C. B. Musgrave, *J. Am. Chem. Soc.*, 2013, **135**, 142–154.
65 65 C. Zinelaabidine, O. Souad, J. Zoubir, B. Malika and A. Nour-Eddine, *Int. J. Chem.*, 2012, **4**, 73–79.
66 66 S. Strasser and C. Slugovc, *Catal. Sci. Technol.*, 2015, **5**, 5091–5094.
67 67 S. I. Matsuoka, S. Namera and M. Suzuki, *Polym. Chem.*, 2015, **6**, 294–301.
68 68 S. Strasser, C. Wappl and C. Slugovc, *Polym. Chem.*, 2017, **8**, 1797–1804.
69 69 H. Yang, Y. Zuo, J. Zhang, Y. Song, W. Huang, X. Xue, Q. Jiang, A. Sun and B. Jiang, *Polym. Chem.*, 2018, **9**, 4716–4723.
70 70 N. S. Shaikh, V. H. Deshpande and A. V. Bedekar, *Tetrahedron*, 2001, **57**, 9045–9048.
71 71 M. K. Chaudhuri, S. Hussain, M. L. Kantam and B. Neelima, *Tetrahedron Lett.*, 2005, **46**, 8329–8331.
72 72 A. V. Marenich, C. J. Cramer and D. G. Truhlar, *J. Phys. Chem. B*, 2009, **113**, 6378–6396.
73 73 D. Allgauer, H. Jangra, H. Asahara, Z. Li, Q. Chen, H. Zipse, R. O. Armin and H. Mayr, *J. Am. Chem. Soc.*, 2017, **139**, 13318–13329.
74 74 L.-G. Zhou, W. Liao and Z.-X. Yu, *Asian J. Org. Chem.*, 2012, **1**, 336–345.
75 75 R. G. Parr, L. V. Szentpály and S. Liu, *J. Am. Chem. Soc.*, 1999, **121**, 1922–1924.
76 76 D. S. Allgäuer, H. Jangra, H. Asahara, Z. Li, Q. Chen, H. Zipse, A. R. Ofial and H. Mayr, *J. Am. Chem. Soc.*, 2017, **139**, 13318–13329.
77 77 K. Kim, N. R. Singstock, K. K. Childress, J. Sinha, A. M. Salazar, S. N. Whitfield, A. M. Holder, J. W. Stansbury and C. B. Musgrave, *J. Am. Chem. Soc.*, 2019, **141**, 6279–6291.
78 78 Y. Takemoto, *Org. Biomol. Chem.*, 2005, **3**, 4299–4306.
79 79 T. Inokuma, Y. Hoashi and Y. Takemoto, *J. Am. Chem. Soc.*, 2006, **128**, 9413–9419.
80 80 X. Yu and W. Wang, *Chem. Asian J.*, 2008, **3**, 516–532.
81 81 H. C. Kolb, M. G. Finn and K. B. Sharpless, *Angew. Chem. Int. Ed.*, 2001, **40**, 2004–2021.
82 82 C. Laurence, M. Berthelot, U. De Nantes and L. De Spectrochimie, *Perspect. Drug Discov. Des.*, 2000, **18**, 39–60.
83 83 S. H. Hsiao and C. H. Yu, *J. Polym. Sci. Part A Polym. Chem.*, 1998, **36**, 1847–1854.
84 84 G. Métral, J. Wentland, Y. Thomann and J. C. Tiller, *Macromol. Rapid Commun.*, 2005, **26**, 1330–1335.
85 85 M. K. McBride, B. T. Worrell, T. Brown, L. M. Cox, N. Sowan, C. Wang, M. Podgorski, A. M. Martinez and C. N. Bowman, *Annu. Rev. Chem. Biomol. Eng.*, 2019, **10**, annurev-chembioeng-060718-030217.
86 86 M. J. Frisch, G. W. Trucks, H. B. . Schlegel, G. E. . Scuseria, M. A. . Robb, J. R. . Cheeseman, G. . Scalmani, V. . Barone, B. . Mennucci, G. A. . Petersson, H. . Nakatsuji, X. . Caricato, M.; Li, H. P. . Hratchian, A. F. . Izmaylov, G. . Bloino, J.; Zheng, D. J. Sonnenb, M. . Hada, M. . Ehara, K. . Toyota, R. . Fukuda, J. . Hasegawa, M. . Ishida, T. . Nakajima, Y. . Honda, O. . Kitao, H. . Nakai, T. . Vreven, J. A. . Montgomery, Jr., J. E. . Peralta, F. . Ogliaro, M. . Bearpark, J. J. . Heyd, E. . Brothers, K. N. . Kudin, V. N. . Staroverov, R. . Kobayashi, J. . Normand, K. . Raghavachari, A. . Rendell, J. C. . Burant, S. S. . Iyengar, J. . Tomasi, M. . Cossi, N. . Rega, N. J. . Millam, M. . Klene, J. E. . Knox, J. B. . Cross, V. . Bakken, C. . Adamo, J. . Jaramillo, R. . Gomperts, R. E. . Stratmann, O. . Yazyev, A. J. . Austin, R. . Cammi, C. . Pomelli, J. W. . Ochterski, R. L. . Martin, K. . Morokuma, V. G. . Zakrzewski, G. A. . Voth, P. . Salvador, J. J. . Dannenberg and D. J. Dapprich, 2016.
87 87 H. S. Yu, X. He, S. L. Li and D. G. Truhlar, *Chem. Sci.*, 2016, **7**, 5032–5051.
88 88 V. A. Rassolov, M. A. Ratner, J. A. Pople, P. C. Redfern and L. A. Curtiss, *J. Comput. Chem.*, 2001, **22**, 976–984.
89 89 M. Besora, P. Vidossich, A. Lledós, G. Ujaque and F. Maseras, *J. Phys. Chem. A*, 2018, **122**, 1392–1399.
90 90 J. P. Foster and F. Weinhold, *J. Am. Chem. Soc.*, 1980, **102**, 7211–7218.

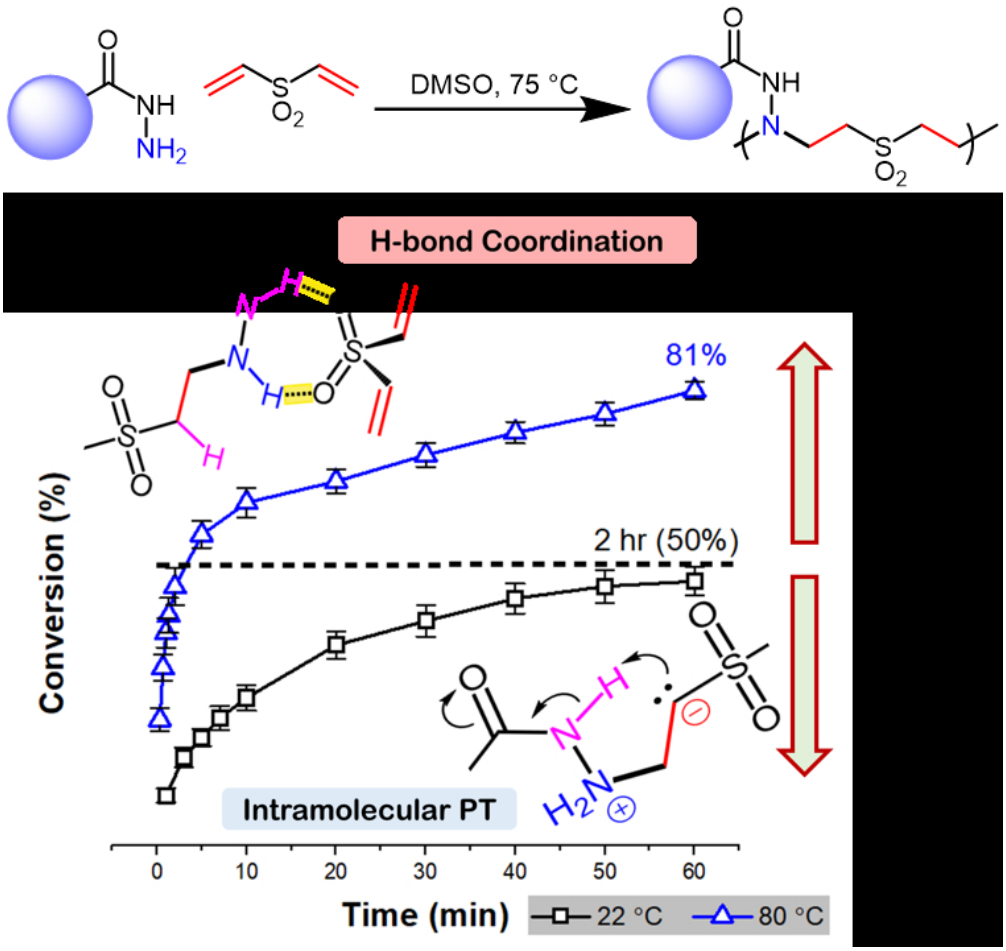

128x121mm (150 x 150 DPI)